Compressive multiple view projection incoherent holography

Authors: Yair Rivenson, Adrian Stern, and Joseph Rosen
Publication: Optics Express, 2011
Speaker: Sangjun Park

Short summary: In this seminar, the principles of the multiple view projection (MVP) holography technique are given. After understanding the principles, the intuition of the paper is shortly given. Finally, the new technique so called compressive multiple view projection (CMVP) holography is presented and the numerical simulations are also demonstrated.

I. INTRODUCTION

1. Holography is a classical method to store three dimensional information of a scene.
2. Acquisition methods of traditional holography are required high coherence and high powered sources such as lasers.
3. Without using the sources, the multiple view projection (MVP) holography technique is proposed.
4. The authors have pointed the drawback of the MVP holography technique, and then they have remedied the drawback by adopting the compressive sensing (CS) approach.

II. THE MULTIPLE VIEW PROJECTION (MVP) HOLOGRAPHY TECHNIQUE

1. According to the paper, the MVP holography technique appears to solve the traditional Holography technique that requires the sources such as lasers.

2. The process of the MVP holography technique:
   A. While a digital camera moves, it captures many view of the same scene from different angles.
   B. Each captured scene is projected into the CCD plane.
   C. Then, the different projections are used to synthesize a digital hologram.

3. Any ordinal digital camera can be used to store a three dimensional information of a scene.
4. The drawback of the MVP holography technique requires a significant scanning effort.
   A. For example, to generate a hologram whose size is 256×256, $256 \times 256 = 65536$ projections are acquired.

5. To remedy the drawback, techniques [Rosen07][Kim10] have been proposed.
   A. The first one is to employ a lenslet array instead of the CCD plane. But, this approach gives a low resolution hologram. [Kim10]
   B. The second one is to reduce scanning times by recording only a small number of the projections and synthesizing the rest using a view synthesis stereo algorithm. But, this approach faces with some difficulties in handling multiple scenes. [Rosen07]
   C. Please, read the papers if you have interested in them (They are not covered in this seminar). According to the authors, the proposed technique in this paper remedies the drawbacks presented in the papers.

6. The process of obtaining a digital hologram using the MVP technique is divided into optical and digital stages according to the paper.
   A. In the optical stage, different perspectives of the scene obtaining from a digital camera are recorded.

i. The perspective can be characterized by a pair of angles (φ_m, θ_n).

ii. The $(m,n)^{th}$ projection is denoted to $p_{mn}(x_p, y_p)$, where x_p and y_p are the coordinates in the projection domain.

B. In the digital stage, we multiply each acquired projection by a complex phase function $f_{mn} = \exp\{-j2\pi b(x_p \sin\varphi_m + y_p \sin\theta_n)\}$, where b is a real constant.

C. Obtaining a Fourier hologram. It is done by integrating the product of p_{mn} and f_{mn} as following: $h(m,n) = \iint p_{mn}(x_p, y_p) f_{mn} dx_p dy_p$. Then, we obtain a complex scalar for every projection (φ_m, θ_n).

i. By taking a Fourier transform on $h(m,n)$, we will get a reconstruction which corresponds only to $z = 0$ plane of the scene.

ii. In general, to obtain a reconstruction corresponding to z_i, we should multiply the hologram by a quadratic phase function. Viz.

$$u_i(x,y) = \mathcal{F}^{-1}\left\{h(v_x, v_y)\exp\left[-j\pi\lambda z_i\left(v_x^2 + v_y^2\right)\right]\right\}, \quad (1)$$

where u_i is the reconstructed plane, both v_x and v_y indicate spatial frequencies, λ denotes the central wavelength and $\mathcal{F}$ represents the Fourier transform.

D. Since digital holograms are considered, (1) becomes

$$u_i(x,y) = \sum_m \sum_n h(m,n)\exp\left\{-j\pi\lambda z_i\left[(\Delta v_x m)^2 + (\Delta v_y n)^2\right]\right\}\exp\left\{j2\pi\left(\frac{mp}{N_x} + \frac{nq}{N_y}\right)\right\}, \quad (2)$$

where N_x and N_y are the number of pixels in the x and y directions respectively. For simplicity, $N_x = N_y = N$. (2) can be rewritten as a matrix-vector multiplication form as following:

$$\mathbf{u}_i = \mathbf{F}^{-1}\mathbf{Q}_{-\lambda^2 z_i}\mathbf{h}, \tag{3}$$

where $\mathbf{u}_i$ is a $N^2 \times 1$ vector corresponding to z_i plane. Let F be a $N \times N$ discrete Fourier transform matrix whose elements are $F_{m,p} = \exp(-j2\pi mp/N)$. Then, $\mathbf{F} = F \otimes F \in \mathbb{C}^{N^2 \times N^2}$, where $\otimes$ is the Kronecker product. The matrix $\mathbf{Q}_{-\lambda^2 z_i} \in \mathbb{C}^{N^2 \times N^2}$ is a diagonal matrix with quadratic phase elements along its diagonal.

E. Shortly, reconstructing $\mathbf{u}_i$ is easy. $\mathbf{F}$ is given, $\mathbf{Q}_{-\lambda^2 z_i}$ is determined the angles, and $\mathbf{h}$ is obtained by integrating the product of p_{mn} and f_{mn}.

F. To understand how to get $\mathbf{h}$ from an experiment, we need to read the following papers.[Rosen01][Rosen03]…

III. Compressive Sensing approach for reducing the number of projections

1. The idea is very simple and intuitive.

   A. To reconstruct a hologram, what things do we need? They are $\mathbf{F}$, $\mathbf{Q}_{-\lambda^2 z_i}$ and $\mathbf{h}$.

   B. Among them, what is the measured factor in an experiment? It is $\mathbf{h}$.

2. The authors assume that the synthesized Fourier hologram $\mathbf{h}$ can be sparse. Then, this assumption allows us to reduce the size of $\mathbf{h}$. It is the main idea of this paper.

3. Let us denote $\mathbf{h}^M$ to the subsampled Fourier hologram. By solving the below equation

$$\hat{\mathbf{u}}_i = \arg\min_{\mathbf{u}_i} \left\{ \left\| \mathbf{u}_i - \mathbf{F}^{-1}\mathbf{Q}_{-\lambda^2 z_i}\mathbf{h}^M \right\|_2^2 + \gamma \left\| \Psi_i \mathbf{u}_i \right\|_1 \right\}, \tag{4}$$

we can reconstruct an object plane $\mathbf{u}_i$ at distance z_i from $z=0$ plane. In the paper, the authors recommend Ψ_i such as Haar wavelet or total variation and the authors name it compressive multiple view projection (CMVP) holography.

IV. SUMMARY OF THE CMVP HOLOGRAPHY

1. Instead of $N^2 = N_x \times N_y$ projections, only $\Omega(K \log N)$ random projections of the scene are taken.
2. Multiply each taken projection p_{mn} by its corresponding phase function f_{mn}.
3. Then, we get a single Fourier hologram by doing $h(m,n) = \iint p_{mn}(x_p, y_p) f_{mn} dx_p dy_p$.
4. After obtaining an under-sampled Fourier hologram $\mathbf{h}^M$, we can reconstruct each plane of the scene by solving (4).

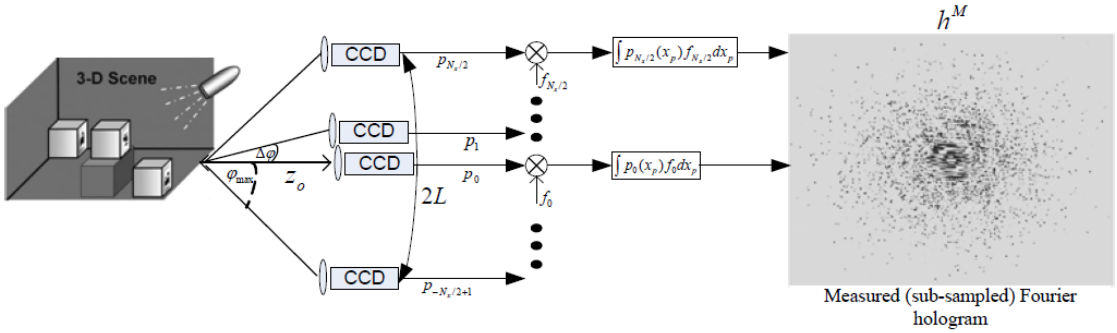

Fig. 1. Illustration of CMVP hologram acquisition. Acquisition of only $\approx K \log N_x$ projections results in a heavily undersampled Fourier hologram. Each sample in the hologram plane corresponds to a nonuniformly randomly picked projection.

In the above Fig. 1, the CMVP hologram acquisition is shown. For simplicity, only a scan along the *x*-axis is shown. The minimal angular distance between two adjacent projections is $\Delta\varphi$, and z_0 is the distance between the imaging system and the object. The length of the CCD's translation trajectory is $2L$.

V. NUMERICAL RESULTS

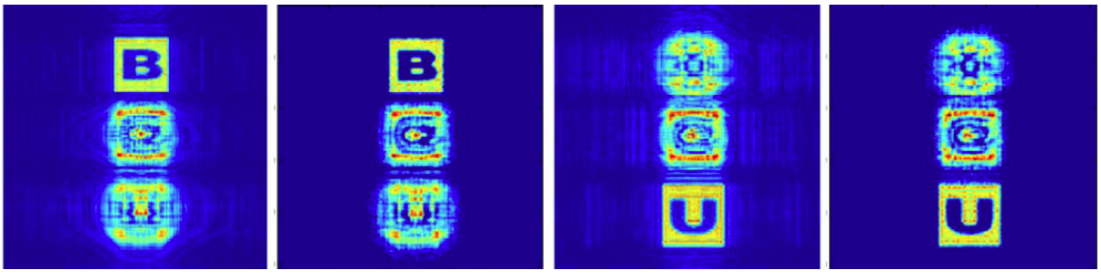

(a) (b) (c) (d)

Fig. 2. Reconstruction examples of the B and U planes of simulated data. (a) Reconstruction of the B plane from 100% of the projections. (b) CS reconstruction of the B plane from 6% of the projections. (c) Reconstruction of the U plane from 100% of the projections. (d) CS reconstruction of the U plane from 6% of the projections.

In both (a) and (c), 256×256 projections are required.

In both (b) and (d), $256 \times 256 \times 0.06$ projections are acquired.

In the CMVP method, Haar wavelet transform is used and TwIST solvers is used to solve (4).

VI. CONCLUSION

1. In this paper, the authors shortly have summarized about the multiple view projection (MVP) holography technique (See Section 2). Then, the authors have proposed the compressive multiple view projection (CMVP) technique (See Section 3).
2. The strong advantages of the proposed technique are that 1) it does not require changing a sensing hardware, 2) it gives a high resolution hologram compared to the previous technique [Kim10], and 3) it does not require a distinct anchor point problem arisen in [Rosen07].

   (In the paper, the authors have made a part System's Resolution Analysis for the theoretical analysis of the system's resolution limit. If you have interested in it, please carefully read the paper)

   (The distinct anchor point problem is that the technique [Rosen07] requires the distinct anchor points to interpolate the different perspectives of the scene. Thus, if the scene is changed, then the distinct anchor points are also changed. However, the CMVP technique is free from this)

VII. DISCUSSION

After meeting, please write discussion in the meeting and update your presentation file.

Reference

[Rosen01] Y. Li, D. Abookasis, and J. rosen, “Computer-generated holograms of three-dimensional realistic objects recorded without wave interference,” Appl. Opt. 40(17), 2864 – 2870 (2001).

[Rosen03] D. Abookasis, and J. Rosen, “Computer-generated holograms of three-dimensional objects synthesized from their multiple angular viewpoints, “J. Opt. Soc. Am. A 20(8), 1537 – 1545 (2003).

[Rosen07] B. Katz, N. T. Shaked, and J. Rosen, “Synthesizing computer generated holograms with reduced number of perspective projections,” Opt. Express 15(20), 13250 – 13255 (2007).

[Kim10] N. Chen, J.-H. Park, and N. Kim, “Parameter analysis of integral Fourier hologram and its resolution enhancement,” Opt. Express 18(3), 2152 – 2167 (2010).

Compressed Sensing of EEG for Wireless Telemonitoring with Low Energy Consumption and Inexpensive Hardware

Authors: Zhilin Zhang, Tzyy-Ping Jung, Scott Makeig, Bhaskar D. Rao,
Publication: IEEE TRANSACTIONS ON BIOMEDICAL ENGINEERING, 2012
Speaker: Younghak Shin

Short summary: Telemonitoring of electroencephalogram (EEG) through wireless body-area networks (WBAN) is an evolving direction in personalized medicine. However, there are important constraints such as energy consumption, data compression, and device cost. Recently, Block Sparse Bayesian Learning (BSBL) was proposed as a new method to the CS problem. In this study, they apply the technique to the telemonitoring of EEG. Experimental results show that its recovery quality is better than state-of-the-art CS algorithms. These results suggest that BSBL is very promising for telemonitoring of EEG and other non-sparse physiological signals.

I. INTRODUCTION

Telemonitoring of electroencephalogram (EEG) via WBANs is an evolving direction in personalized medicine and home-based e-Health. Equipped with the system, patients need not visit hospitals frequently. Instead, their EEG can be monitored continuously and ubiquitously.

However, there are many constraints

A. The primary one is energy constraint. Due to limitation on battery life, it is necessary to reduce energy consumption as much as possible.

B. Another constraint is that transmitted physiological signals should be largely compressed.

C. The third constraint is hardware costs. Low hardware costs are more likely to make a telemonitoring system economically feasible and accepted by individual customers

It is noted that many conventional data compression method such as wavelet compression cannot satisfy all the above constraints at the same time.

Compared to wavelet compression, Compressed Sensing (CS) can reduce energy consumption while achieving competitive data compression ratio.

However, current CS algorithms only work well for sparse signals or signals with sparse representation coefficients in some transformed domains (e.g., the wavelet domain).

Since EEG is neither sparse in the original time domain nor sparse in transformed domains, current CS algorithms cannot achieve good recovery quality.

This study proposes using Block Sparse Bayesian Learning (BSBL) [1] to compress/recover EEG. The BSBL framework was initially proposed for signals with block structure. This study explores the feasibility of using the BSBL technique for EEG, which is an example of a signal without distinct block structure.

II. COMPRESSED SENSING AND BLOCK SPARSE BAYESIAN LEARNING

CS is a new data compression paradigm, in which a signal of length *N*, denoted by $\mathbf{x} \in \mathbb{R}^{M \times N}$, is compressed by a full row-rank random matrix, denoted by $\mathbf{\Phi} \in \mathbb{R}^{M \times N}$ $\left(M \ll N\right)$,i.e.,

$$\mathbf{y} = \mathbf{\Phi x}, \tag{1}$$

where $\mathbf{y}$ is the compressed data, and $\mathbf{\Phi}$ is called the *sensing matrix*. CS algorithms use the compressed data $\mathbf{y}$ and the sensing matrix $\mathbf{\Phi}$ to recover the original signal $\mathbf{x}$. Their successes rely on the key assumption that most entries of the signal x are zero (i.e., $\mathbf{x}$ is sparse).

When this assumption does not hold, one can seek a dictionary matrix, denoted by $\mathbf{D} \in \mathbb{R}^{M \times M}$, so that $\mathbf{x}$ can be expressed as $\mathbf{x} = \mathbf{Dz}$ and $\mathbf{z}$ is sparse.

$$\mathbf{y} = \mathbf{\Phi D z}. \tag{2}$$

When CS is used in a telemonitoring system, signals are compressed on sensors according to (1). This compression stage consumes on-chip energy of the WBAN. The signals are recovered by a remote computer according to (2). This stage does not consume any energy of the WBAN.

Despite of many advantages, the use of CS in telemonitoring is only limited to a few types of signals, because most physiological signals like EEG are not sparse in the time domain and not sparse enough in transformed domains.

The issue now can be solved by the BSBL framework [1], [2].

It assumes the signal **x** can be partitioned into a concatenation of non-overlapping blocks, and a few of blocks are non-zero. Thus, it requires users to define the block partition of **x**.

However, it turns out that user-defined block partition does not need to be consistent with the true block partition [3]. Further, in this work, they found even if a signal has no distinct block structure, the BSBL framework is still effective.

This makes feasible using BSBL for the CS of EEG, since EEG has arbitrary waveforms and the representation coefficients **z** generally lack block structure.

Currently, there are three algorithms in the BSBL framework. In this experiment, they chose a bound-optimization based algorithm, denoted by BSBL-BO. Details on the algorithm and the BSBL framework can be found in [1].

III. EXPERIMENTS OF COMPRESSED SENSING OF EEG

The following experiments compared BSBL-BO with some representative CS algorithms in terms of recovery quality.

Two performance indexes were used to measure recovery quality. One was the Normalized Mean Square Error (NMSE). The second was the Structural SIMilarity index (SSIM) [4]. SSIM measures the similarity between the recovered signal and the original signal, which is a better performance index than the NMSE for structured signals.

In the first experiment **D** was an inverse Discrete Cosine Transform (DCT) matrix, and thus **z** $\left(\mathbf{z}=\mathbf{D}^{-1}\mathbf{x}\right)$ are DCT coefficients. In the second experiment **D** was an inverse Daubechies-20 Wavelet Transform (WT) matrix.

In both experiments the sensing matrices $\mathbf{\Phi}$ were sparse binary matrices, in which every column contained 15 entries equal to 1 with random locations while other entries were zeros.

A. Experiment 1: Compressed Sensing with DCT

This example used a common dataset (‘eeglab data.set’) in the EEGLab. This dataset contains

EEG signals of 32 channels with sequence length of 30720 data points, and each channel signal contains 80 epochs each containing 384 points.

To compress the signals epoch by epoch, they used a 192 ×384 sparse binary matrix as the sensing matrix $\mathbf{\Phi}$, and a 384×384 inverse DCT matrix as the dictionary matrix **D**.

Two representative CS algorithms were compared in this experiment. One was the Model-CoSaMP, which has high performance for signals with known block structure. The second was an L1 algorithm (CVX toolbox) to recover EEG.

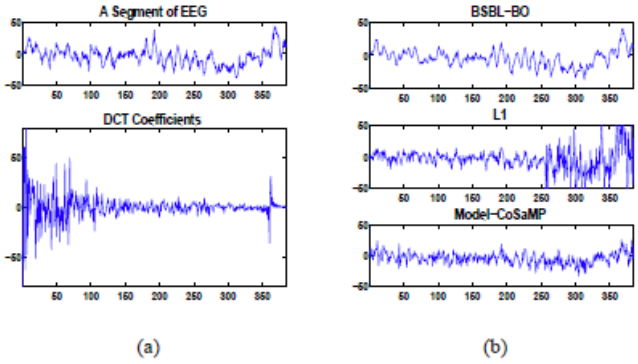

Fig. 1. (a) An EEG epoch, and its DCT coefficients. (b) The recovery results by BSBL-BO, ℓ_1, and Model-CoSaMP when using the model (2).

Figure 1(a) shows an EEG epoch and its DCT coefficients. Clearly, the DCT coefficients were not sparse and had no block structure. Figure 1(b) shows the recovery results of the three algorithms. BSBL-BO recovered the epoch with good quality.

Table I shows the averaged NMSE and SSIM of the three algorithms on the whole dataset.

TABLE I
AVERAGED PERFORMANCE IN EXPERIMENT 1.

	NMSE (mean ± std)	SSIM (mean ± std)
DCT-based BSBL-BO	**0.078 ± 0.046**	**0.85 ± 0.08**
BSBL-BO without DCT	0.116 ± 0.066	0.81 ± 0.09
DCT-based ℓ_1	0.493 ± 0.121	0.48 ± 0.11
DCT-based Block-CoSaMP	0.434 ± 0.070	0.45 ± 0.10

The DCT-based BSBL-BO evidently had the best performance.

B. Experiment 2: Compressed Sensing with WT

The second experiment used movement direction dataset. It consists of multiple channel signals, each channel signal containing 250 epochs for each of two events ('left direction' and 'right direction'). BSBL-BO and the previous L1 algorithm were compared.

The sensing matrix $\mathbf{\Phi}$ had the size of 128 × 256, and the dictionary matrix D had the size of 256 × 256.

For each event, they calculated the ERP by averaging the associated 250 recovered epochs.

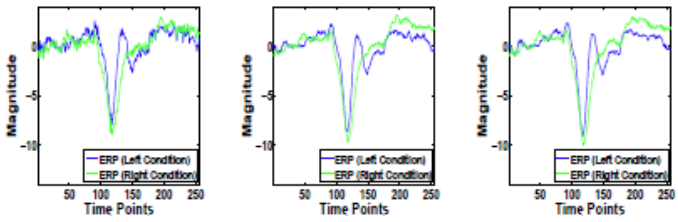

Fig. 3. The ERPs corresponding to two event conditions ('left' and 'right') averaged (a) from the recovered epochs by the ℓ_1 algorithm, (b) from the recovered epochs by BSBL-BO, and (c) from the original dataset.

Figure 3 (a) shows the ERP for the 'left direction' and the ERP for the 'right direction' averaged from the dataset recovered by the L1 algorithm. Figure 3 (b) shows the ERPs from the recovered dataset by BSBL-BO. Figure 3 (c) shows the ERPs from the original dataset.

Clearly, the resulting ERPs by the L1 algorithm were noisy.

The ERPs averaged from the recovered by BSBL-BO maintained all the details of the original ERPs with high consistency. The SSIM and the NMSE of the resulting ERPs by the L1 algorithm were 0.92 and 0.044, respectively. In contrast, the SSIM and the NMSE of the resulting ERPs by BSBL-BO were 0.97 and 0.008, respectively.

IV. DISCUSSIONS

Using various dictionary matrices, the representation coefficients of EEG signals are still not sparse. Therefore, current CS algorithms have poor performance, and their recovery quality is not suitable for many clinical applications and cognitive neuroscience studies.

Instead of seeking optimal dictionary matrices, this study proposed a method using general dictionary matrices achieving sufficient recovery quality for typical cognitive neuroscience studies.

The empirical results suggest that when using the BSBL framework for EEG compression/recovery, the seeking of optimal dictionary matrices is not very crucial.

V. CONCLUSIONS

This study proposed to use the framework of block sparse Bayesian learning, which has superior performance to other existing CS algorithms in recovering non-sparse signals. Experimental results showed that it recovered EEG signals with good quality. Thus, it is very promising for wireless telemonitoring based cognitive neuroscience studies.

VI. DISCUSSION & COMMENTS

This method can be applied other research area with non-sparse signal.

Appendix

Experiment codes can be downloaded at:

https://sites.google.com/site/researchbyzhang/bsbl.

Reference

[1] Z. Zhang and B. D. Rao, "Extension of SBL algorithms for the recovery of block sparse signals with intra-block correlation," IEEE Trans. On Signal Processing (submitted), 2012.

[2] ——, "Sparse signal recovery with temporally correlated source vectors using sparse Bayesian learning," IEEE Journal of Selected Topics in Signal Processing, vol. 5, no. 5, pp. 912–926, 2011.

[3] Z. Zhang, T.-P. Jung, S. Makeig, and B. D. Rao, "Low energy wireless body-area networks for fetal ECG elemonitoring via the framework of block sparse Bayesian learning," IEEE Trans. on Biomedical Engineering (submitted), 2012.

[4] Z. Wang and A. Bovik, "Mean squared error: Love it or leave it? a new look at signal fidelity measures," IEEE Signal Processing Magazine, vol. 26, no. 1, pp. 98–117, 2009.

Compressive sensing in medical ultrasound (Invited paper)

H. Liebgott et al.

IEEE Intl. Ultrasonics Symp. (2012. July)

Presenter : Jin-Taek Seong

GIST, Dept. of Information and Communications, INFONET Lab.

Gwangju Institute of Science and Technology

Introduction

- Compressed sensing can be applied for two main purposes:
  - *i*) it can lower the amount of data needed and thus allows to speed up acquisition.
  - An example in the field of medical imaging of such application is dynamic MRI [4].
  - *ii*) it can improve the reconstruction of signals/images in fields where constraints or the physical acquisition set up yields very sparse data sets.
  - A typical example is seismic data recovery in geophysics [5].
- The objective of this paper is
  - to give the reader an overview of the different attempts to show the feasibility of CS in medical ultrasound.
- The classification of the studies is done according to the data that are considered to be sparse.
  - the scatterer distribution itself, the pre-beamforming channel data, the beamformed RF signal and even Dopple data.

Introduction

- The way that how to be sparse in some domains is a key idea to apply the inverse problem to the CS problem.
- In this paper, they show several schemes that expand data into sparse signals.

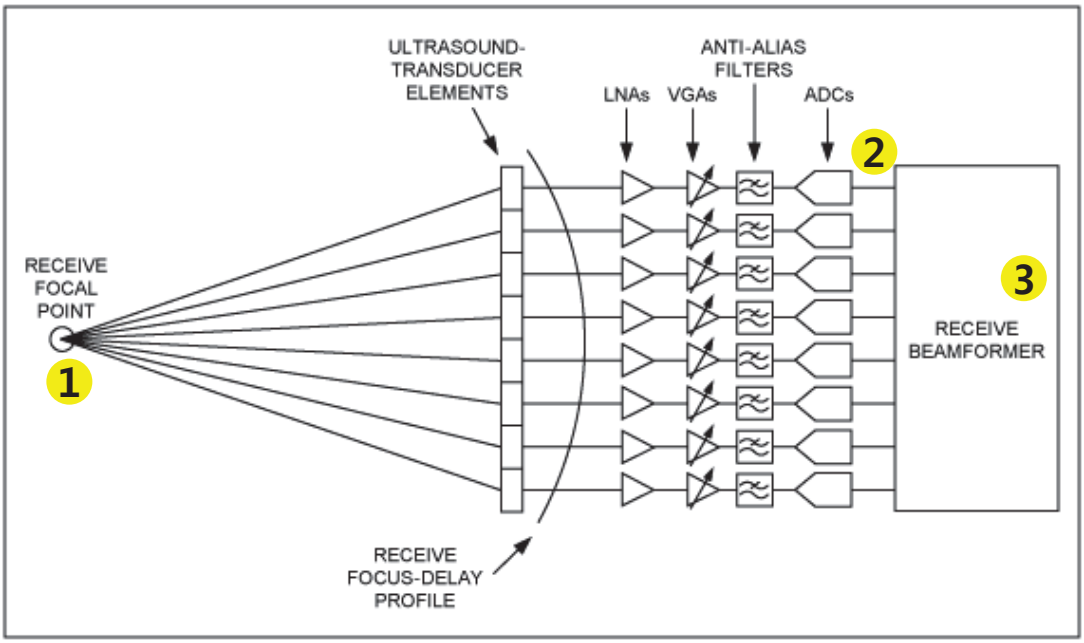

Application to Ultrasound Imaging

- A central concern in CS is that the data under consideration should have sparse expansion in some dictionaries.
  - Fourier basis, wavelet basis, dictionary learned from data, etc...
  - i.e., the number of non-zero coefficients of the image or signal in this representation basis should be as small as possible.
- One of the main features of the existing studies is the type of signal/image to be reconstructed and the choice of the representation where the US data are assumed to be sparse.
- We overview the following models in the sparse domains
  - Sparse diffusion map
  - Sparse Raw RF
  - Sparse assumption of the RF images Fourier transform
  - Doppler imaging

Sparse diffusion map

- Several groups of authors [12-18] have chosen to model the medium under investigation itself as a sparse distribution of scatters.
- However, considering that most of the scatters have an echogenecity close to zero is more unusual.
- The basic idea [12-13] is to write the direct scattering problem and solve the inverse problem under the constraint that the scatter distribution is sparse.

$$\boldsymbol{p}^{sc}\left(e_\theta\right)=\boldsymbol{G}\left(e_\theta\right)\gamma_K$$

  - With $\boldsymbol{p}^{sc}\left(e_\theta\right)$ the scattered pressure received by the transducer elements after transmission of a plane wave in direction θ, $\boldsymbol{G}\left(e_\theta\right)$ represents propagation and interaction with the scatters and γ_K is the scatter distribution lying on a regular grid.
- If γ_K is assumed to be sparse, this problem is equivalent to the CS problem.

Sparse diffusion map

- Figure shows a result from a simple phantom consisting in four isolated scatters obtained with this approach.

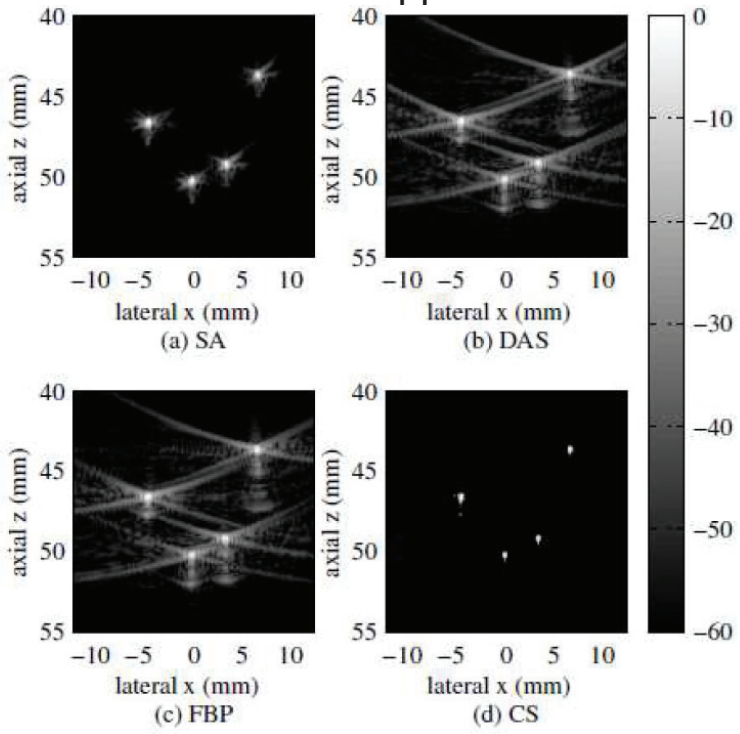

  - The CS result (d) is compared with synthetic aperture (a), delay and sum (b) and Fourier propagation (c).

Sparse diffusion map

- With the same assumption [14, 15] proposed another approach based on finite rate of innovation and Xampling.

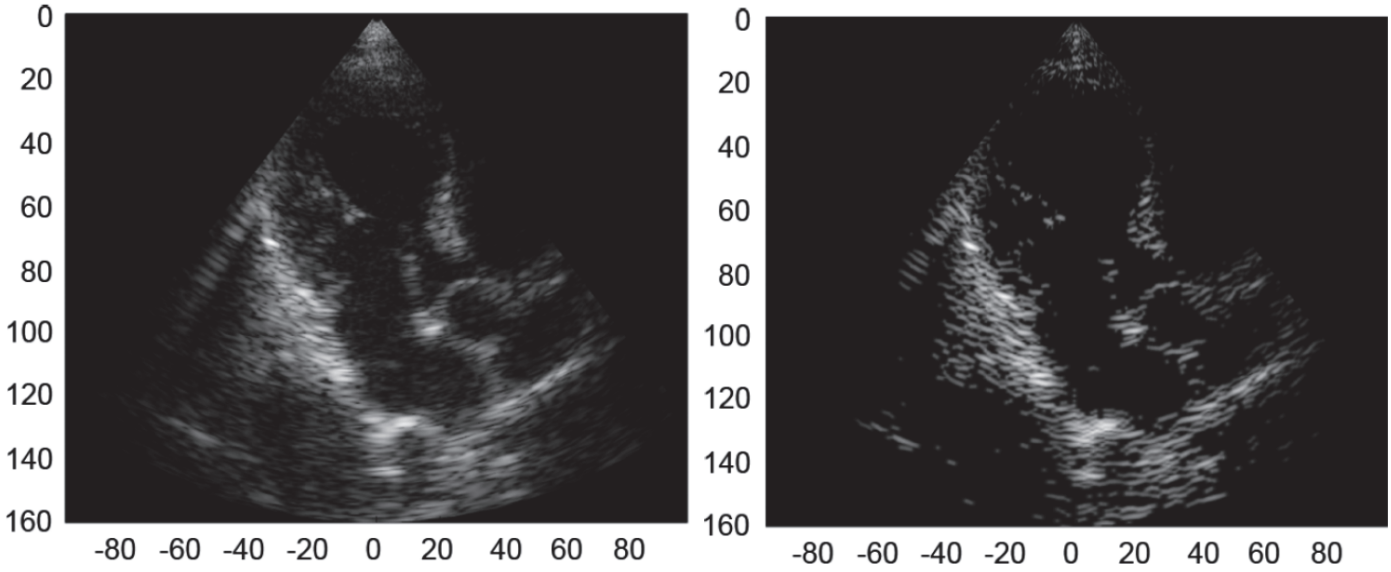

- The edges are well reconstructed but the speckle is close to be completely lost in some parts of the images.
- This is consistent assumption of scatter map sparsity.

Sparse Raw RF

- Another group of authors [21-24] consider that the raw channel data gathered at each transducer element during receive have a sparse decomposition in some basis.
- The objective of such an approach is to reduce the quantity of pre-beamformed data acquired and evaluate the ability of this approach to reconstruct B-mode images of good quality.

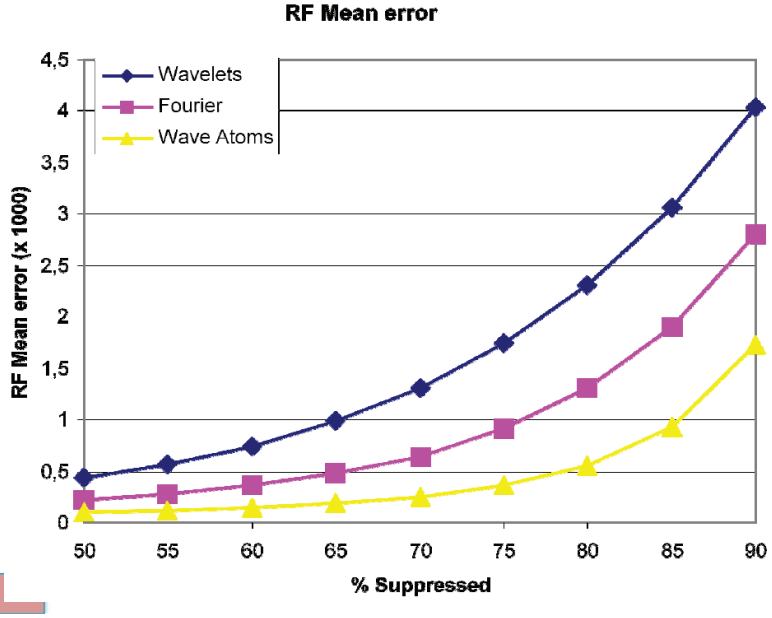

Sparse Raw RF

- Figure shows experimental results obtained from only 20% of the original data using CS and wave atoms.

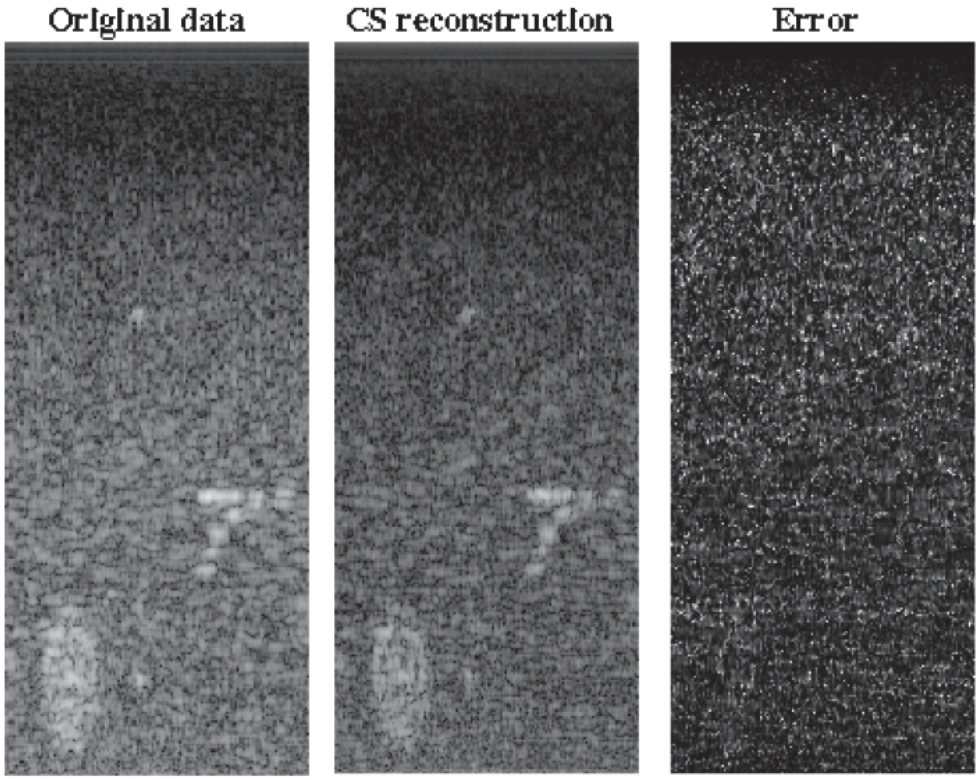

Sparse assumption of the RF images Fourier transform

- The reconstruction of post-beamforming 2D RF images via CS technique is addressed.
- The sparsity assumption is related to the assumption of bandlimited RF signal acquisition.
- The 2D Fourier transform of RF images is assumed to be sparse.

$$y = \Phi \Psi x$$

  - Φ denotes the sampling mask, Ψ is the 2D Fourier Transform.

Random post-beamforming RF sampling mask

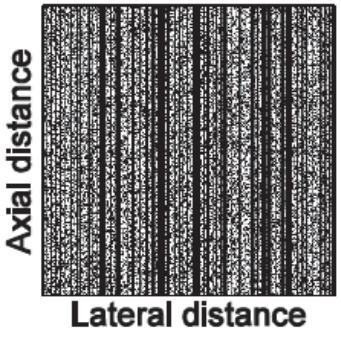

Sparse assumption of the RF images

- (a) original simulated RF image, (b) RF samples used for reconstruction, (c) reconstructed RF image using a reweighted conjugate gradient optimization, (d) reconstructed RF image using the Bayesian framework proposed in [20].

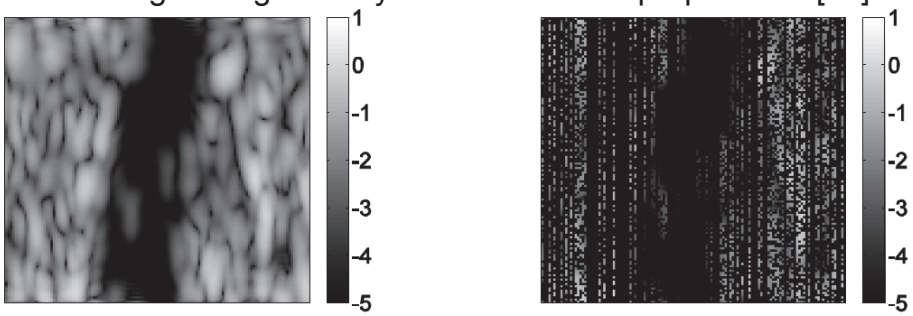

(a) (b)

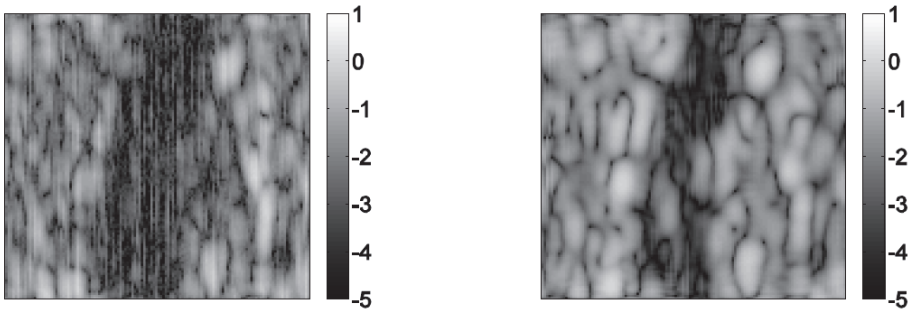

(c) (d)

Doppler imaging

- CS has also been proposed for Doppler imaging [32, 33].
- The authors [32] made the assumption that the Fourier transform of the Doppler signal is sparse.

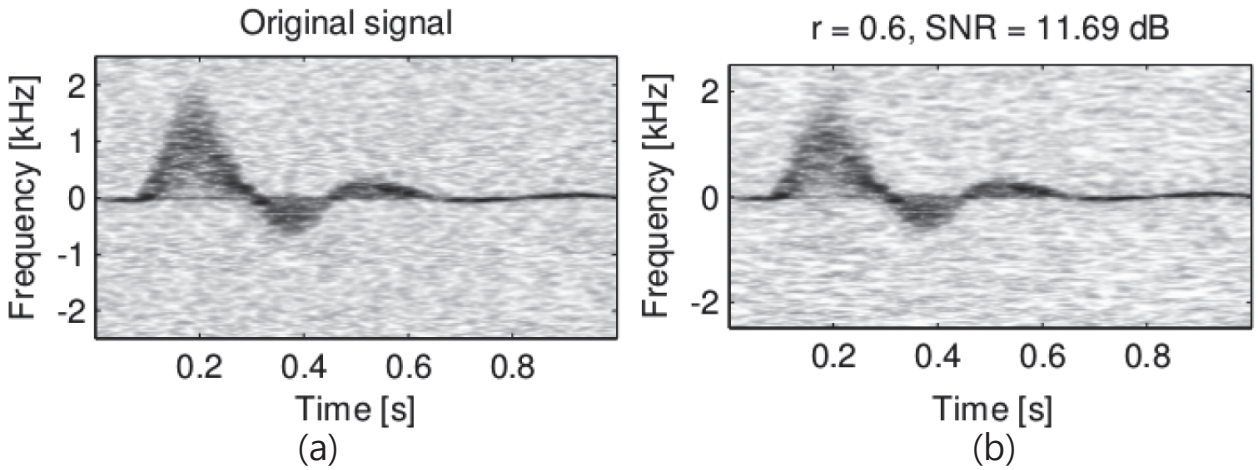

- In vivo Doopler result from a femoral artery. (a) real sonogram; (b) reconstructed sonogram based on CS, where r is the ratio of the number of Doppler samples to the total number of samples.

Conclusion

- Compressed sensing medical ultrasound is a very recent field of research that can lead to drastic modifications in the way ultrasound scanners are developed.
- The technique is feasible but far from its technological applicability.
- The key points for CS to work are
  - A sparsifying basis
  - A measure basis in coherent with the sparsifying basis
  - Dedicated acquisition material
  - Fast and robust reconstruction algorithms
- Improvements are necessary for all of these concerns.
- Efforts should be made in order to maintain the real-time characteristic of medical ultrasound.

Reference

- [4] M. Lustig, D. Donoho, and J. M. Pauly, “Sparse MRI: The application of compressed sensing for rapid MR imaging,” Magnetic Resonance in Medicine, vol. 58, pp. 1182-1195, 2007.
- [5] F. J. Herrmann and G. Hennenfent, “Non-parametric seismic data recovery with curvelet frames,” Geophysical Journal Intl., vol. 173, pp. 223-248, 2008.

Enhanced performance by a hybrid NIRS–EEG brain computer interface.

Siamac Fazli et al. (Benjamin Blankertz*)

NeuroImage (2012)

Presenter : SeungChan Lee

GIST, Dept. of Information and Communication, INFONET Lab.

Gwangju Institute of Science and Technology

Background

- NIRS
  - Near-infrared spectroscopy (NIRS) is a spectroscopic method that uses the near-infrared region of the electromagnetic spectrum.
  - NIRS measures the concentration changes of oxygenated and deoxygenated hemoglobins ([HbO] and [HbR]) in the superficial layers of the human cortex.
  - While concentration of [HbO] is expected to increase after focal activation of the cortex due to higher blood flow, [HbR] is washed out and decreases.

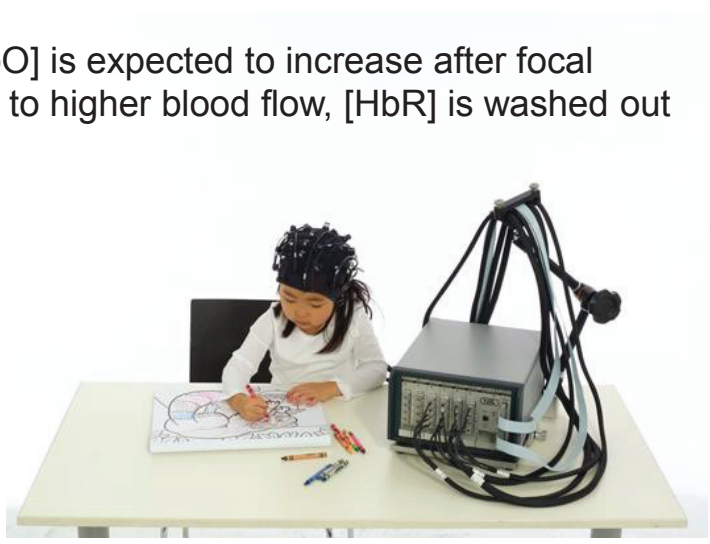

Introduction & Motivation

- Hybrid BCI approach
  - For increasing information transfer rates and robustness of the classification
  - Combination of EEG features from multiple domains such as movement related potentials (MRPs) and event-related desynchronizations (ERD).
  - Combinations of EEG and peripheral parameters such as electromyography(EMG), electrooculogram(EOG)
- Limitation in neuroimaging techniques
  - EEG : spatial resolution
  - NIRS, fMRI : temporal resolution
- Goals
  - Implement a hybrid BCI by extracting relevant NIRS features to support and complement high-speed EEG-based BCI.
  - Evaluate the time delay and spatial information content of the hemodynamic response and show enhance and robust BCI performance during a SMR-based BCI paradigm.

Experiment design

- Data acquisition
  - NIRS system : NIRScout 8–16 (NIRx Medizintechnik GmbH, Germany)
    - 24 optical fibers (8 sources with wavelengths of 850 nm and 760 nm, 16 detectors convolving to 24 measurement channels)
    - The sampling rate is 6.25Hz
  - EEG system : BrainAmp (Brain Products, Munich, Germany)
    - 37 Ag/AgCl electrodes, 2 bipolar EMG, 2 bipolar EOG
    - The sampling rate is 1kHz and downsampled to 100 Hz.
  - The optical probes are constructed such that they fit into the ring of standard electrodes.

Experiment design

- Locations of electrodes

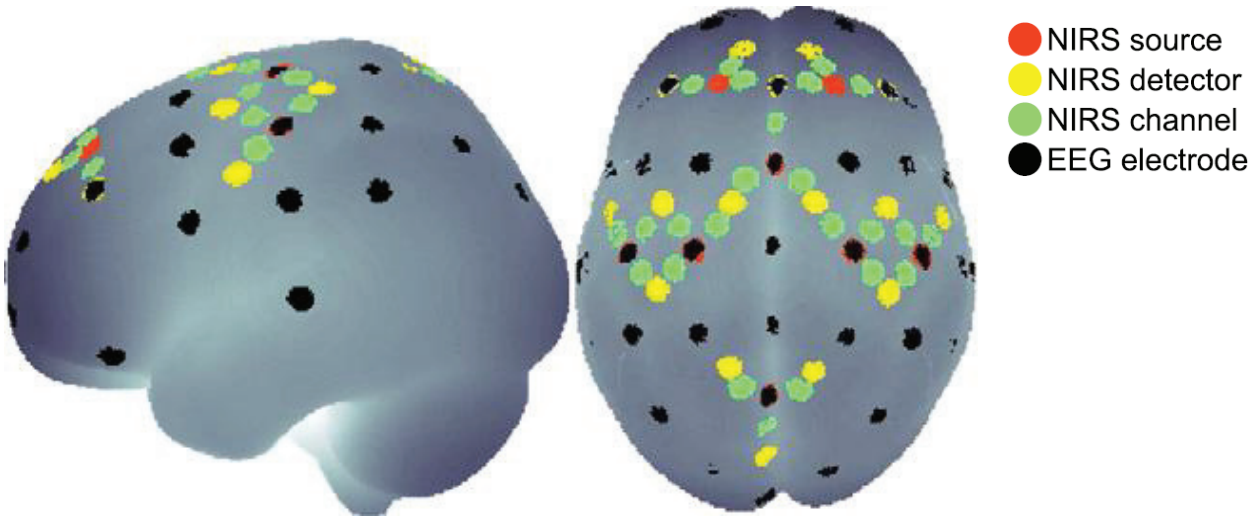

Experiment design

- Experiment design
  - 14 healthy, right-handed volunteers (aged 20 to 30)
  - 2 class motor function(left vs. right hand movements)
  - 2 blocks of motor execution by means of hand gripping (24 trials per block per condition) and 2 blocks of real-time EEG-based, visual feedback controlled motor imagery (50 trials per block per condition)
    - first 2s : trial began with a black fixation cross
    - 2 ~ 6s : visual cue an arrow appeared pointing to the left or right
    - 2 ~ 6s motor imagery : the fixation cross started moving for 4 s according to the classifier output
    - After 4s : blank screen for 10.5±1.5 s.

Data analysis

- EEG analysis
  - Offline analysis + Motor imagery of feedback session based on ***coadaptive calibration***
  - First block of 100 trials : subject-independent classifier (band power estimates of laplacian filtered from motor-related EEG channels)
  - Second block of 100 trials : subject-dependent spatial and temporal filters were estimated from the data of the first block and combined with some subject-independent features
  - Feedback features(moving cross) were calculated every 40 ms with a sliding window of 750 ms.

Data analysis

- NIRS analysis
  - Only offline analysis based on Lamber-beer law
  - Low-pass filtered at 0.2Hz(3rd order Butterworth-filter)
  - A mean of baseline interval(−2s ~ 0s) subtracted from each trial.
  - Average over the time length of the moving window width

Data analysis

- Classification
  - -6 ~ 15 seconds data and moving window (width 1 s, step size=500 ms) are used for classification.
  - 8-fold cross validation with Linear discriminant analysis (LDA).

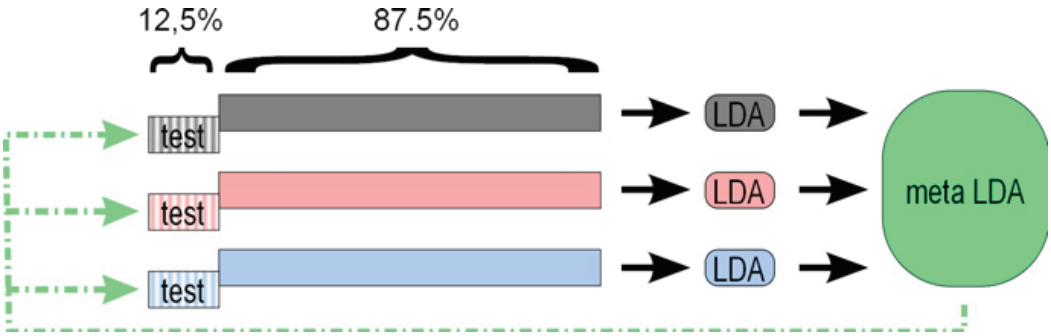

  - 78 training data and 18 test data (real movements)
  - An individual LDA classifier is computed for EEG, [HbO] and [HbR]
  - A meta-classifier is estimated for optimally combining the three LDA outputs.
  - All LDA classifiers are then applied to the test set

Results

- Comparison of classification accuracies and peak classification time
  - For showing the physiological reliability of NIRS feature classification both in time and location.

Accuracies	Real	Imagery
EEG	90.8%	78.2%
HbO	71.1%	71.7%
HbR	73.3%	65.0%

Peak clas.	Real	Imagery
EEG	1680±1014ms	1430±707ms
HbO	7430±2201ms	6501±1579ms
HbR	6966±2484ms	6109±1339ms

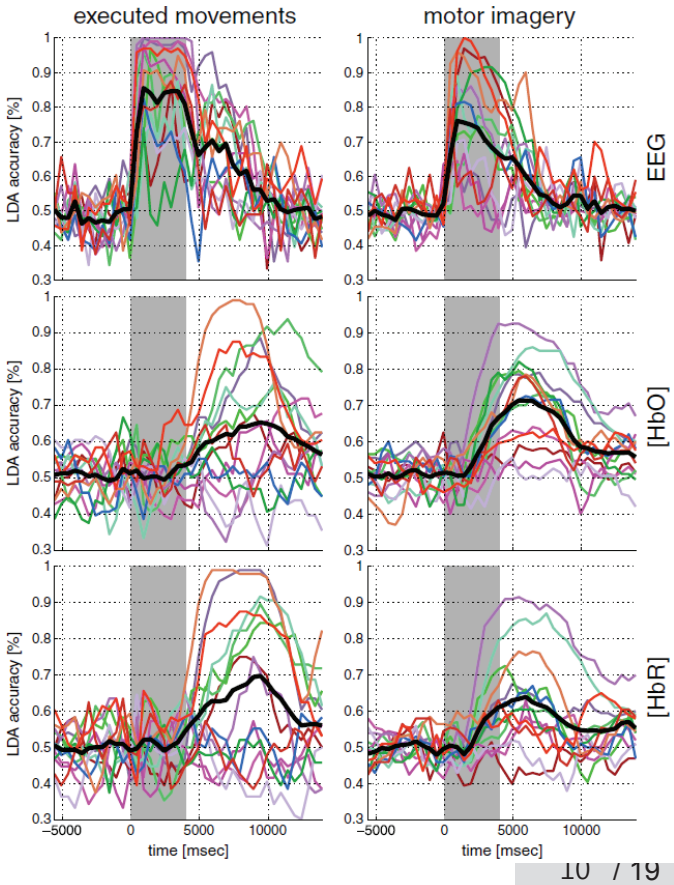

Results

- Topology of significant EEG and NIRS features
  - Motor execution

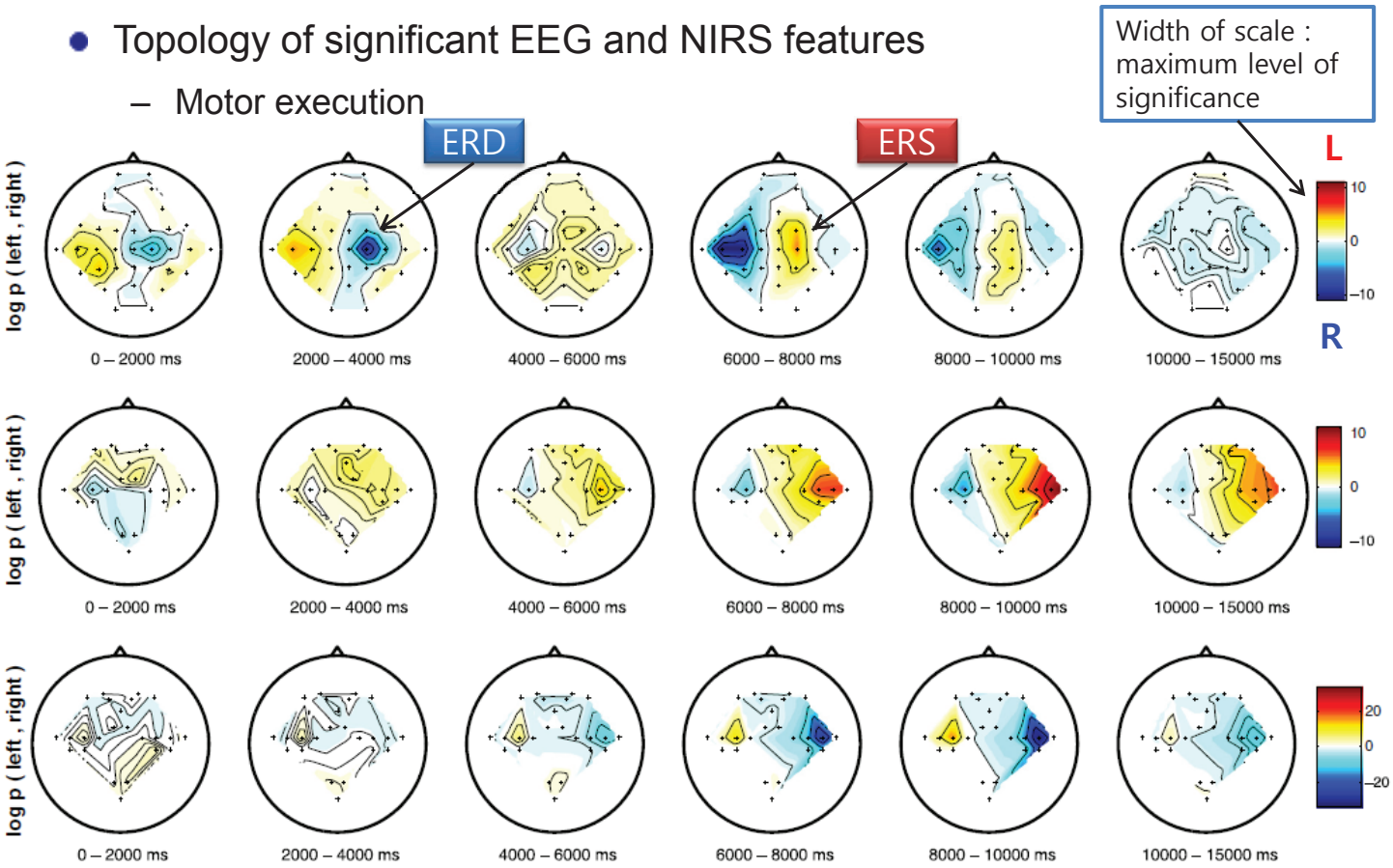

Results

- Topology of significant EEG and NIRS features
  - Motor imageries

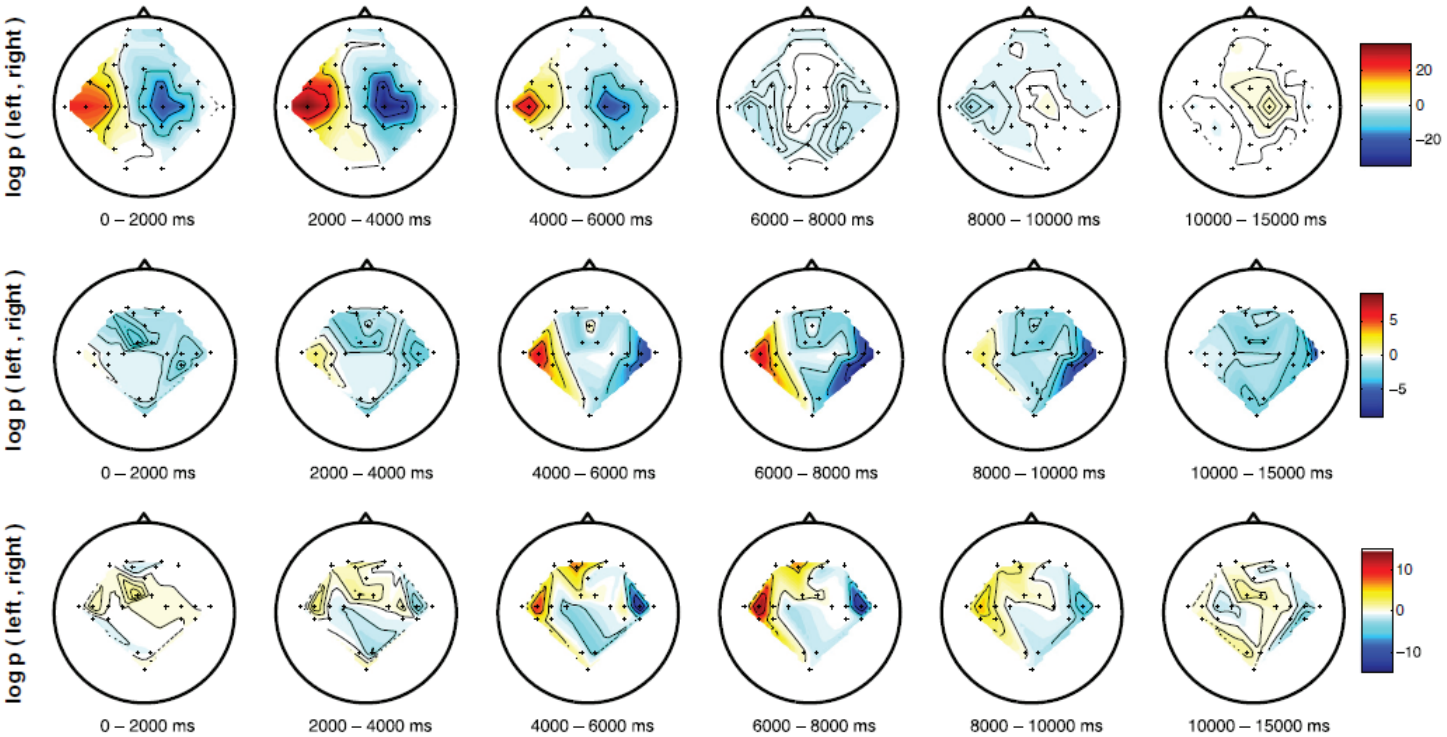

Results

- Topology of significant EEG and NIRS features
  - They found higher significance levels of [HbR] in both paradigms, but [HbO] yielded higher accuracies for motor imagery.
  - They found the inverted polarity of [HbO] for motor imagery.

Results

- Individual LDA classification accuracies for each measurement methods with a meta-classifier
  - A meta classifier was derived for combining the individual signals.
  - Only combinations of measured features for motor imagery score shown (highly) significant improvements.
    - When comparing EEG with combined EEG/[HbO] for motor imagery, there was an average 5% classification accuracy increase across all subjects.

Mean Accuracies	Real	Imagery
EEG	90.8%	78.2%
HbO	71.1%	71.7%
HbR	73.3%	65.0%
EEG+HbO	92.6%	83.2%
EEG+HbR	93.2%	80.6%
EEG+HbO+HbR	87.4%	83.1%

Red latter : Highly significant improvements based on paired t-test

Results

- Scatter plot comparing classification accuracies and significance values of various combination methods
  - Hybrid approaches are effective for motor imagery

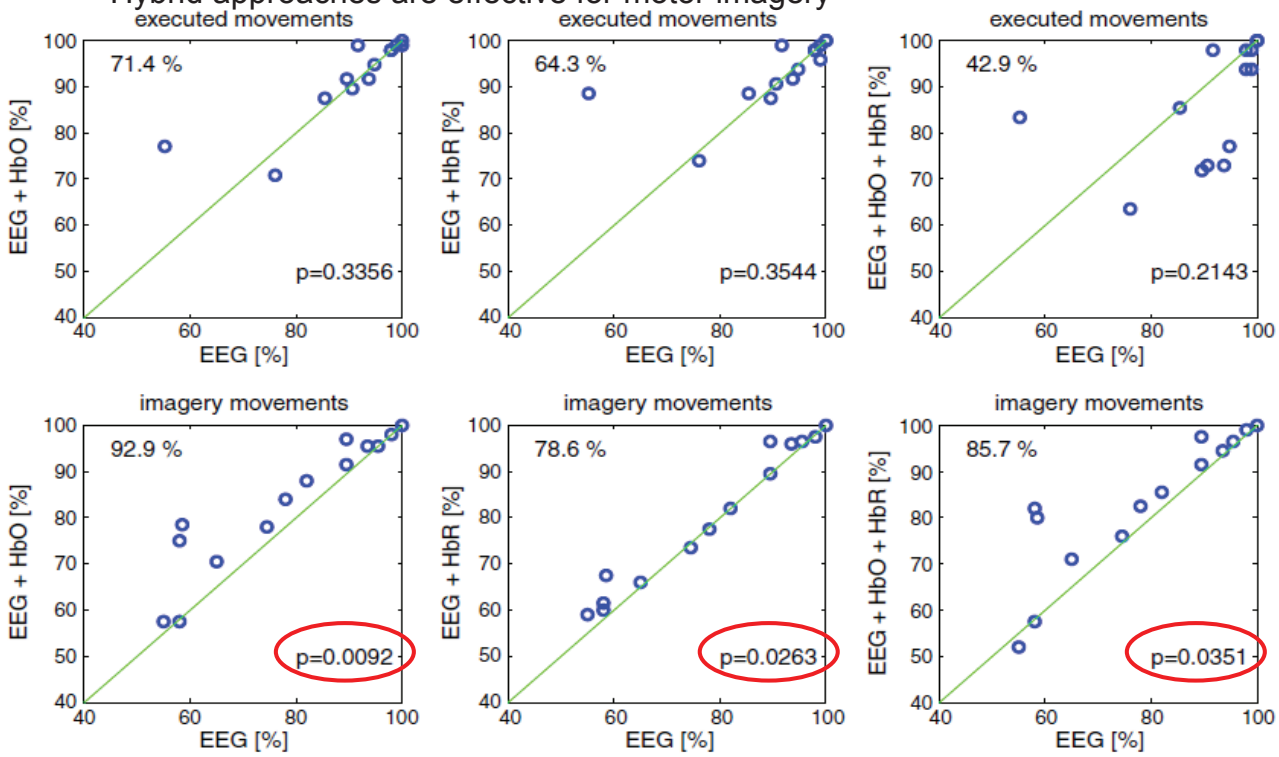

Results

- Mutual information vs. accuracy

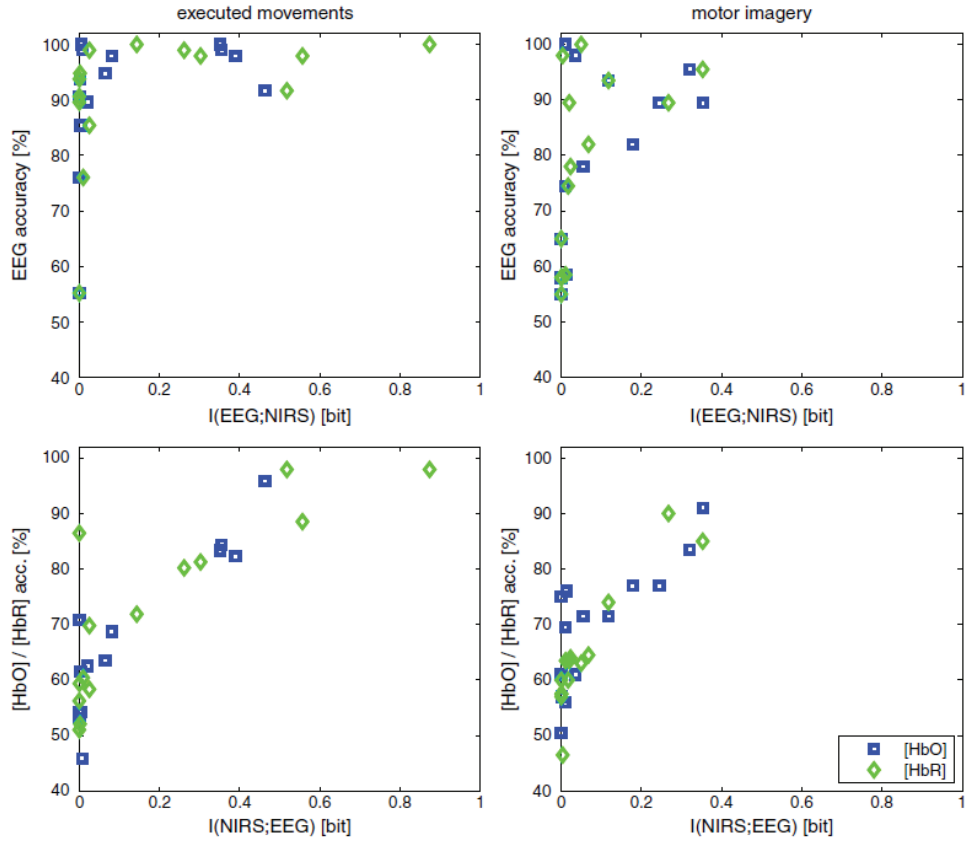

Results

- Mutual information vs. accuracy
  - Relation of the classification performance (y-axes) of the individual measurement methods (EEG, [HbO] and [HbR]) in relation to their mutual information content (I(EEG; [HbO]) and I(EEG; [HbR]) (x-axes).
  - Generally, mutual information is directly proportional to accuracy
    - If for a given subject method X scores a low classification accuracy, one would expect the conditional entropy H(X|Y) to be of similar magnitude as H(X) and therefore the mutual information content is very low.
  - While the classification accuracy of a given method is high, we observe a low mutual information content.
    - the other classification method does not work well
    - their information content is complementary
  - Average mutual information over all subjects

Mutual information	Real	Imagery
I(EEG:HbO)	0.125±0.177bit	0.096±0.127bit
I(EEG:HbR)	0.194±0.277bit	0.067±0.110bit

Conclusion

- In a combination with EEG, they find that NIRS is capable of enhancing event-related desynchronization (ERD)-based BCI performance significantly.
- Behaviors of HbO and HbR
  - Typical behavior of hemoglobin oxygenation during brain activation consists of an increase in [HbO] approximately mirrored by a decrease of [HbR]
  - For motor imagery, only [HbR] clearly showed the typical behavior but [HbO] there seems to be an initial drop followed by a subsequent rise
- Limitation of NIRS based BCI
  - long time delay of the hemodynamic response
  - Advantages
    - For subjects (and patients) which are not able to operate a BCI, solely based on EEG, this combination presents a viable alternative.
    - One could imagine a feedback scenario, where a secondary NIRS-derived classifier is only turned on in particular trials, when the 'primary' EEG-based classification is likely to fail.

Discussion

- Evaluation of hybrid NIRS–EEG brain computer interface
  - Hybrid measurement is helpful in classification of SMR based BCI
  - Classification of NIRS response is not higher than EEG based BCI
  - Long time delay of the hemodynamic response lead to lower information transfer rate
  - There is no benefit with hybrid NIRS-EEG based BCI yet
- Probable research direction
  - Hybrid NIRS-EEG based BCI with real time classification
  - Zero training classifier and adaptive calibration with real time experiment